JOURNAL OF SOLID STATE CHEMISTRY **122,** 376–383 (1996)
ARTICLE NO. 0130

Synthesis, Crystal Structure, Electrical, Magnetic, and Electrochemical Lithium Intercalation Properties of Vanadium Oxynitrides[1]

B. Wang, B. C. Chakoumakos, B. C. Sales, and J. B. Bates

Solid State Division, Oak Ridge National Laboratory, P.O. Box 2008, Oak Ridge, Tennessee 37831-6030

Received September 29, 1995; accepted December 20, 1995

Polycrystalline vanadium oxynitrides have been prepared by heat-treating V_2O_5 at high temperature in a flowing ammonia atmosphere. Single-phase cubic samples, with the rock salt structure, were produced by nitridation at 600–700°C. Powder diffraction data from neutrons at two wavelengths and Cu$K\alpha$ X-rays of these oxynitrides were analyzed using the Rietveld method, but strong correlation among the atomic displacement parameters, site occupancies, and the N/O ratio did not allow a refinement of unique compositions. Measured densities and cell volumes were used to limit the possible compositional space for each sample, and these were further limited by the charge neutrality requirement. The electrical resistivity of the single-phase sample is about 2×10^{-3} $\Omega \cdot$ cm and is weakly temperature dependent below room temperature. Magnetic susceptibility measurements show no evidence of magnetic ordering and yield a magnetic moment of 0.25 μ_B per V atom. Electrochemical lithium intercalation measurements indicate that only a small concentration of lithium ions were inserted into the cathode due to the close-packed NaCl structure of cubic vanadium oxynitride.

INTRODUCTION

A number of vanadium oxides have been recently studied because of their special accommodation to lithium insertion reactions (1–5). Thin film lithium batteries based on amorphous V_2O_5 cathodes have been investigated in this laboratory for several years (6, 7), and it has been found that the IR loss in these batteries is due to slow lithium ion diffusion in the cathode. In an attempt to improve lithium ion transport, we have investigated the structure and physical properties of vanadium oxynitrides as potential cathode materials with the idea that the formation of mixed-valence vanadium will increase the ionic and electronic conductivity. Cathode materials with high conductivity will reduce the internal IR loss and improve battery performance. Metal oxynitrides are also of great interest as advanced catalysts because dual active sites are presented by the metal and the oxygen. The metallic functions include hydrogenation and dehydrogenation of hydrocarbons whereas the acidic functions include isomerization and cracking (8, 9).

Structure–composition relationships have been previously reported for the vanadium oxynitrides (10, 11). Potorochin *et al.* (10) have studied the compositional limits and the lattice parameters of cubic vanadium oxynitrides. Brauer and Reuther (11) investigated the phase relationships in the V–N–O system by X-ray powder diffraction as a function of pressure. However, there are no reports, to our knowledge, of a systematic study of the structure and physical properties of vanadium oxynitrides. In this paper, we report the synthesis, Rietveld structure analysis, electrical, magnetic, and electrochemical properties of vanadium oxynitrides.

EXPERIMENTAL PROCEDURES

Vanadium oxynitrides were prepared by heat-treating V_2O_5 (Alfa, 99.8%) at 500 to 800°C for 24 to 48 h in flowing anhydrous ammonia (SFC purity, 99.995%). About 10 g of V_2O_5 powder were placed in an alumina boat inside a quartz tube. After heat-treating in ammonia at high temperature, the samples were furnace cooled to room temperature. The product formed was black and pseudomorphic to the original V_2O_5 crystal shapes.

Powder X-ray diffraction (PXRD) measurements were made with a Scintag diffractometer equipped with a high-purity Ge detector using Cu$K\alpha$ radiation. Data were collected in the 2θ range of 10°–70° with a scan rate of 2°/min. X-ray data sets for Rietveld refinements were collected using step scans at 0.02° 2θ and 2-s counting time, over the range 10°–160° 2θ. The density of the samples was measured by using a Penta-Pycnometer PP-6 equipped with a 5-cm^3 sample cell. Helium gas was used for purging

[1] The U.S. Government's right to retain a nonexclusive royalty-free license in and to the copyright covering this paper, for governmental purposes, is acknowledged.

0022-4596/96 $18.00

and as the fluid. Before the measurement, the samples were outgassed by purging for 30 min. The standard deviation of repeated measurements was less than 0.04%. Rutherford backscattering spectrometry (RBS) was used to determine the N/O ratios in the samples.

Neutron diffraction data for vanadium oxynitrides were collected using the HB4 powder diffractometer at the High-Flux Isotope Reactor at ORNL (12). The samples were contained in vanadium cans, and two data sets were collected for each sample at 295 K over the 2θ range from 11° to 135° in steps of 0.05° using wavelengths of 1.4177 and 1.0315 Å. The structural refinements were made with the computer program GSAS (13), using the Rietveld method (14). Because V contributes weakly to the diffracted intensity, combined refinements of the neutron and X-ray data were attempted. Even with this approach, the atomic displacement parameters, site occupancies, and N/O ratios were highly correlated, and a reliable determination of the sample compositions was not possible.

The electrical resistivity measurements were made by the classical four-probe method. Thermoelectric power was also measured on the same samples against a copper standard (15). Samples for these measurements were made by cold pressing finely ground powders into a pellet and sintering the pellet at 500°C in flowing N_2. After sintering, the pellets were cut into thin plates with dimensions of ~4 mm × 8 mm by ~1 mm thick. Silver paint was used for metal contacts. Magnetic susceptibility measurements from 10 to 300 K were made on the single-phase cubic material using a Faraday magnetometer (15).

The electrochemical lithium intercalation properties of the vanadium oxynitride were measured in two lithium cells with (a) liquid electrolyte and (b) thin film solid electrolyte. The cell with liquid electrolyte consisted of a single-phase cubic vanadium oxynitride (700°C/24 h sample) pellet (sintered at 500°C in flowing N_2) as the cathode and lithium metal foil as the anode. The electrodes were separated by an Al_2O_3 fiber paper soaked with an electrolyte of 1*M* $LiClO_4$ in propylene carbonate. The cathode pellet measured about 0.10-cm thick by 1.22 cm in diameter and weighed 351 mg. The cell was placed between stainless steel dies inside a glass tube and held in place with a spring that was compressed when O-ring sealed brass caps were pressed over the ends of the tube. Electrical contact with the cell was made through leads clamped to the brass caps. The contacts were made through a spring load inside the tube. For the thin-film solid electrolyte cell, the cathode consisted of 60 wt% single-phase cubic vanadium oxynitride (700°C/48 h sample), 30 wt% $(PEO)_8LiClO_4$ ionic conducting polymer, and 10 wt% carbon. The materials

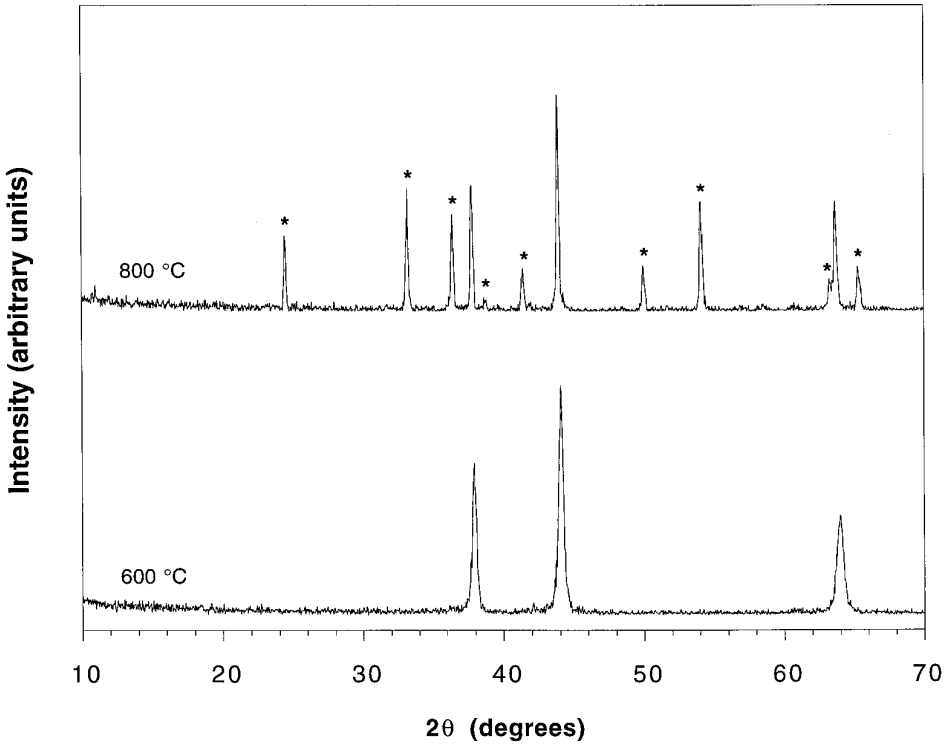

FIG. 1. X-ray powder diffraction patterns (Cu$K\alpha$ radiation) for samples heat-treated in NH_3 at 600 and 800°C for 24 h. The diffraction peaks of the V_2O_3 phase are indicated by asterisks.

were dissolved in acetonitrile to give 3 wt% solution and stirred in a plastic beaker for 24 h. A film of the composite cathode was formed on a 13-mm diameter vanadium disk by spin coating followed by drying at 60°C for 24 h. The thickness of the dried composite cathode measured with a profilometer was 26 μm, and it weighed 13 mg. An approximately 1-μm thick amorphous lithium phosphorus oxynitride electrolyte film was deposited on the top of the cathode by rf magnetron sputtering of Li_3PO_4 in N_2. This material has a typical composition of $Li_{2.9}PO_{3.3}N_{0.46}$ and a conductivity of 2×10^{-6} S · cm^{-1} at 25°C (6). A lithium anode film about 10-μm thick was then deposited at a pressure of about 10^{-6} Torr by evaporation of lithium metal contained in a Ta crucible. The area of the lithium film was 0.54 cm^2, and the corresponding active cathode mass calculated based on this area was 3.2 mg. This assumes that lateral diffusion of lithium in the cathode can be neglected. All the cells were tested in an argon-filled glove box using a 1 mA channel of a Maccor battery test system.

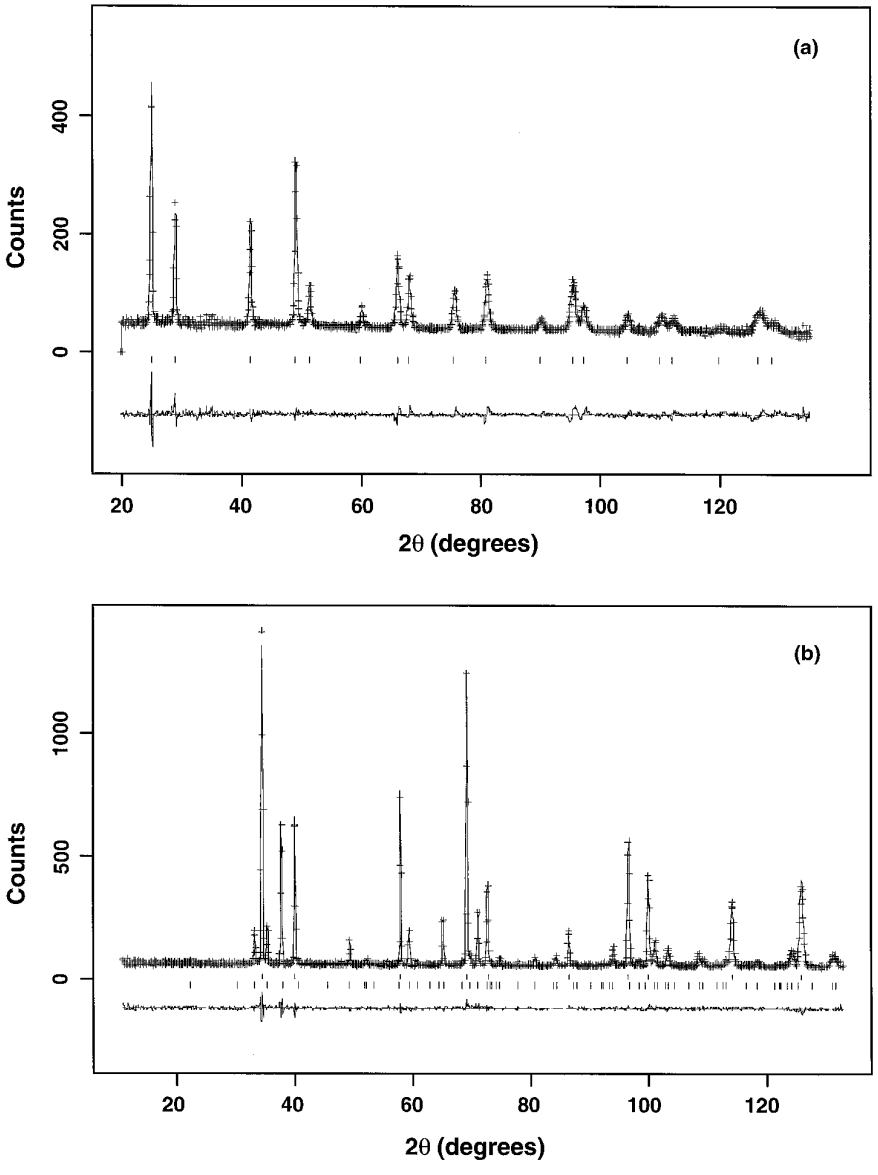

FIG. 2. Observed, calculated, and the difference neutron diffraction profiles for (a) single-phase cubic 600°C/24 h sample (wavelength = 1.0315 Å), and (b) mixed cubic V(O, N) phase and corundum-type V_2O_3 phase sample (wavelength = 1.4177 Å). The observed data are indicated by +, and the calculated profile is the continuous solid line in the same field. The short vertical lines below the profiles mark the positions of all possible Bragg reflections, and the bottom curve is the difference between the observed and calculated intensity plotted using the same vertical scale as the observed and calculated profiles.

TABLE I
Crystal Data and Density Measurements of Vanadium Oxynitrides

Samples	600°C/24 h	700°C/24 h	700°C/48 h	800°C/24 h
Crystal phase	Cubic	Cubic	Cubic	Cubic (84.2 vol%) V_2O_3 (15.8 vol%)
a (Å)	4.12237(8)	4.13439(6)	4.13128(7)	4.13795(8)[a] 4.9541(1),[b] 13.9988(5)[c]
V (Å^3)	70.055(4)	70.670(3)	70.511(4)	70.852(4),[a] 297.55(2)[d]
d_m (g/cm^3)	5.467(4)	5.928(1)	5.677(2)	
Formula Mass (g/mol)[e]	57.672	63.084	60.279	

[a] Cubic phase.
[b] Hexagonal V_2O_3 phase, a (Å).
[c] Hexagonal V_2O_3 phase, c (Å).
[d] Hexagonal V_2O_3 phase.
[e] Calculated by using measured density and cell parameters.

RESULTS AND DISCUSSION

1. Structure and Compositions

X-ray powder patterns show that samples prepared at 600 and 700°C were single phase with the cubic NaCl structure, while the samples heat-treated at 500 and 800°C were mixtures of two phases, the cubic phase and a corundum-type V_2O_3 phase (Fig. 1). Since the ammonia used for nitridation gives both a nitriding and a reducing atmosphere at the heat-treatment temperatures, both the reduction of V^{5+} and the nitridation of V_2O_5 will take place. When the reaction temperature was low, both the reduction and nitridation reactions were slow. Thus, the reaction product was a mixture of the cubic phase and the V_2O_3 phase with the poor crystallinity as confirmed from the X-ray powder diffraction pattern of the 500°C heat-treated sample (not shown). The nitridation reaction was dominant in the temperature range between 600 and 700°C and resulted in single-phase cubic vanadium oxynitrides. However, the reduction reaction was rapid at the higher temperature (800°C) and some V^{5+} was reduced to V^{3+}. Further nitridation of V_2O_3 was difficult due to its high melting point (1760°C). At the same time, the nitridation of V_2O_5 continued to form the cubic phase. Therefore, the overall product at the higher temperature was a mixture of the cubic phase and the V_2O_3 phase with good crystallinity of both phases (Fig. 1).

Examples of the observed, calculated, and difference neutron powder diffraction profiles of the single cubic phase 600°C/24 h sample and the mixed cubic and V_2O_3 phase 800°C/24 h sample are presented in Fig. 2. Full occupancy of the cation and anion sites was assumed in the calculations. Precise cell parameters can be determined from the Rietveld refinement since the cell parameters are not correlated with other structural parameters in the refinement (Table 1). The smaller cell parameter in the 600°C/24 h sample is probably due to a lower cation and anion occupancy in the structure. The high concentration of cation and anion vacancies in cubic NaCl structure has also been observed in other materials such as VO (16).

A summary of the crystal data, measured densities, and formula masses of samples is given in Table I. The refined cell parameters were used with the measured densities to determine the formula mass for each sample. The measured masses of the single cubic-phase samples in this study are smaller than those of the ideal solid solutions VN → VO (64.948 → 66.941 g/mol), which implies that vacancies are present. The formula masses were used to limit the possible compositional space for each of the single cubic

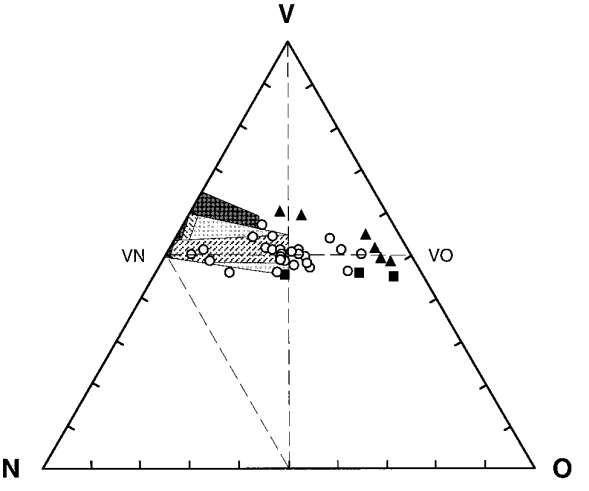

FIG. 3. Phase diagram of V–O–N showing the possible composition regions (light shaded areas) of single-phase cubic vanadium oxynitrides in this study: ▨ 700°C/24 h; ■ 600°C/24 h; ▧ 700°C/48 h, and the compositions studied by Potorochin *et al.* (10): single-phase cubic V(O, N) ○; mixed cubic V(O, N) phase and corundum-type V_2O_3 phase ■; mixed cubic V(O, N) and other hexagonal phase ▲. The dark shaded area shows the single-phase cubic vanadium oxynitride region studied by Brauer and Reuther (11).

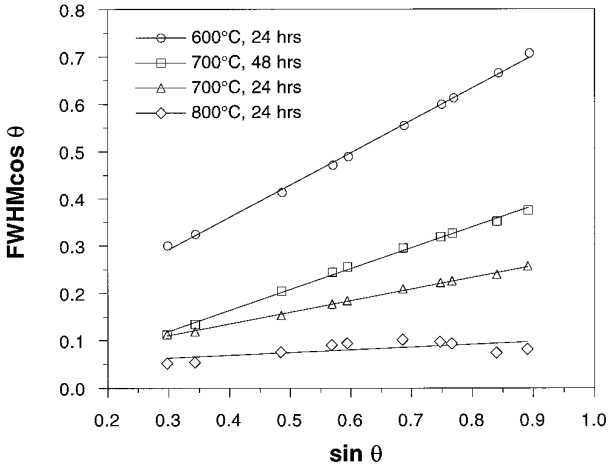

FIG. 4. Full-width-half-maximum (FWHM) as a function of sin θ for the NaCl-type reflections observed in the neutron diffraction data for the vanadium oxynitride samples.

phase samples inside the VN–V–$N_{1/2}O_{1/2}$ region of the V–O–N phase diagram shown in Fig. 3. This region was defined partly by the previous study by Brauer and Reuther (11) and by the RBS results which show that the N/O ratios of samples are >1. The N/O ratios cannot be accurately determined since RBS is a thin-film technique. These single cubic phase regions were further limited by the charge neutrality requirement. The average oxidation state of vanadium was assumed to be between +2 and +3, since these vanadium oxynitrides were black. The possible composition regions of the single cubic phase vanadium oxynitrides of this study displayed in Fig. 3 are in agreement with the composition of vanadium oxynitrides previously reported by Potorochin *et al.* (10) and by Brauer and Reuther (11).

For the mixed cubic and V_2O_3 phase the refined volume fraction (Table 1) indicates that NaCl-type V(O, N) phase is the dominant phase in the sample. Moreover, the refined cell parameters for V_2O_3 match those of pure V_2O_3, suggesting that the N partitions preferentially to the NaCl-type V(O, N) phase.

The full-width-half-maximum (FWHM) as a function of sin θ for the NaCl-type reflections in the neutron diffraction data is shown in Fig. 4. This Williamson–Hall plot has been advocated by Langford *et al.* (17) for rapid assessment of the nature of the peak broadening. The intercept and slope of a Williamson–Hall plot give a qualitative measure of the crystallite size and lattice strain, respectively, where the intercept is inversely proportional to the crystallite size and the slope is directly proportional to the strain. The broadened peaks of the samples were deconvoluted from the instrumental broadening as measured with the NIST standard reference material silicon 640a. From Fig. 4, the intercepts for all temperatures are about the same, so strain appears to be the major contributor to peak broadening rather than a reduction in crystallite size. Furthermore, the strain is significantly relieved as the preparation temperature increases. A possible inconsistency with this analysis is that samples prepared at 700°C showed a greater lattice strain with longer heat treatments. In studies of the catalytic properties of metal oxynitrides, the measured surface areas often exhibit a dependence on the temperature of the ammonolysis, which is interpreted as due to a change in the particle morphology and/or size. In the case of the vanadium oxynitrides studied here, the analysis of the neutron powder diffraction data supports the contention that changes in the particle morphology or size do not contribute to peak broadening in the neutron powder diffraction pattern. The crystallite size, which can be distinctly different from the particle size, remains essentially constant as the processing temperature is varied.

2. Electrical and Magnetic Properties

The temperature dependence of the absolute thermoelectric power and resistivity for the single cubic phase vanadium oxynitride 600°C/24 h sample are shown in Fig. 5. The thermoelectric power is negative and small for the entire temperature range; the magnitude and temperature

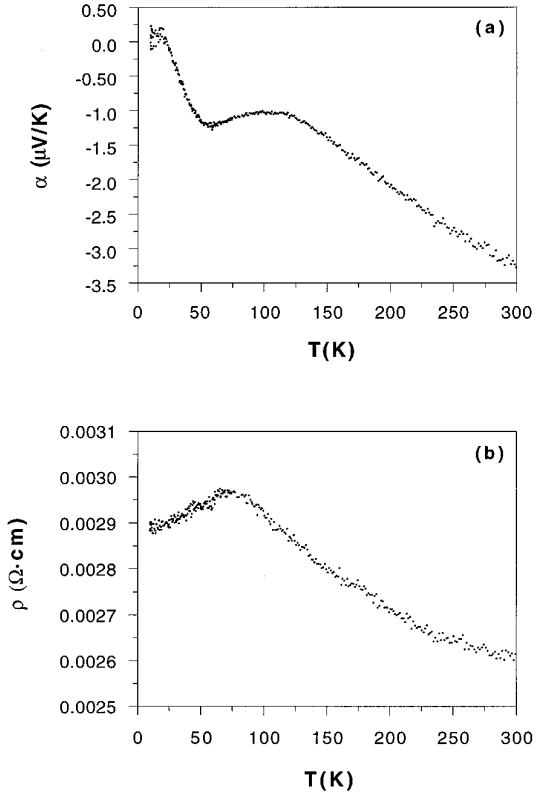

FIG. 5. Thermoelectric power (a) and electrical resistivity (b) as a function of temperature for single-phase cubic vanadium oxynitride 600°C/24 h sample.

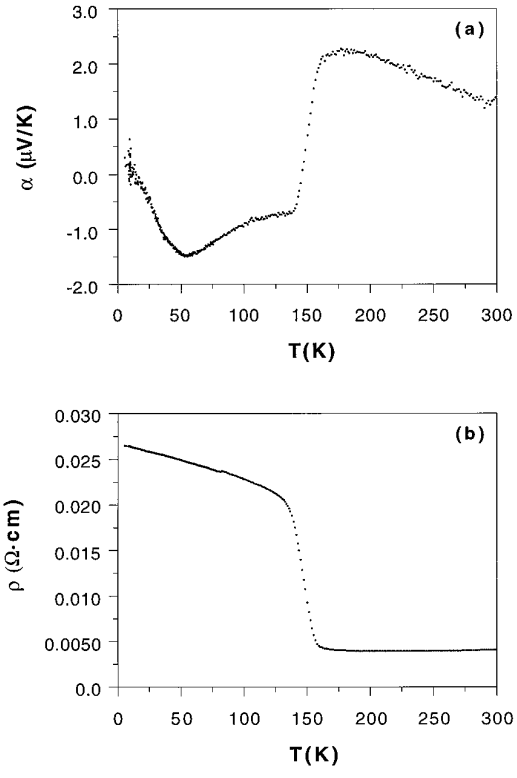

FIG. 6. Thermoelectric power (a) and electrical resistivity (b) as a function of temperature for the mixed cubic V(O, N) phase and V_2O_3 phase 800°C/24 h sample.

dependence are typical for either a metal or a heavily doped semiconductor. The deviation from linearity for temperatures near 60 K is most likely due to phonon drag. The magnitude and sign of the thermopower are indicative of a large number of electrons present in the sample. The weak temperature dependence and magnitude (2×10^{-3} $\Omega \cdot$cm) of the resistivity are characteristic of a heavily doped semiconductor.

The temperature dependence of the thermoelectric power and resistivity for the mixed cubic and corundum V_2O_3 phase sample are similar to that of pure V_2O_3 (Fig. 6). The transition from a metallic to a semiconductive phase is due to a structural phase transition at 170 K from high temperature hexagonal to low temperature monoclinic symmetry (20–23). Neutron diffraction data collected at 12 K on the sample prepared at 800°C also confirmed that a hexagonal to monoclinic structural phase transition occurs. No phase transitions occurred for the single-phase NaCl-type V(O, N) between 293 and 12 K.

The magnetic susceptibility of single-phase NaCl-type 600°C/24 h sample versus $1/T$ is shown in Fig. 7. A well-defined Curie law with a temperature-independent constant term is found for temperatures between 10 and 300 K:

$$\chi = \chi_0 + C/T$$

A least-squares fit of χ_0 and C to the experimental data gives $\chi_0 = 1.5 \times 10^{-4}$ emu/mol and $C = 7.8 \times 10^{-3}$ K · emu/mol. An effective magnetic moment of 0.25 μ_B per vanadium was calculated from these fitting results ($\mu = \sqrt{3k_BC/N}$; k_B is the Boltzmann constant and N is the Avogadro constant). This rather small effective moment suggests that the magnetism likely arises from a small fraction (about 10%) of the total number of vanadium atoms since for typical V^{2+} and V^{3+} compounds the effective moments are 2.8 and 3.8 μ_B, respectively (22).

3. Lithium Intercalation

A cycle of discharge and recharge of the lithium cell based on the single-phase cubic vanadium oxynitride cathode with the liquid electrolyte is shown in Fig. 8. The small specific capacity of the cell corresponds to about 0.02 Li inserted into the cubic vanadium oxynitride cathode during the discharge between 3.5 and 1.5 V. This is significantly smaller than the ~3 Li inserted into V_2O_5 on the first discharge between 3.5 and 1.5 V (6, 7). The insertion of smaller amounts of lithium into the structure of cubic vanadium oxynitride compared to V_2O_5 can be attributed to the differences in the crystal structures. The layered structure of V_2O_5 is favorable for the lithium insertion: VO_5 square pyramids share edges and corners to form layers along the c axis (1, 2). Lithium ions can be inserted into sites between these layers while preserving the V_2O_5 structure (1–5). The close-packing of cations and anions in the NaCl structure of the cubic vanadium oxynitride limits the insertion of lithium ions and leads to the low capacity of the cell. The capacity of the cell with the thin film solid electrolyte is

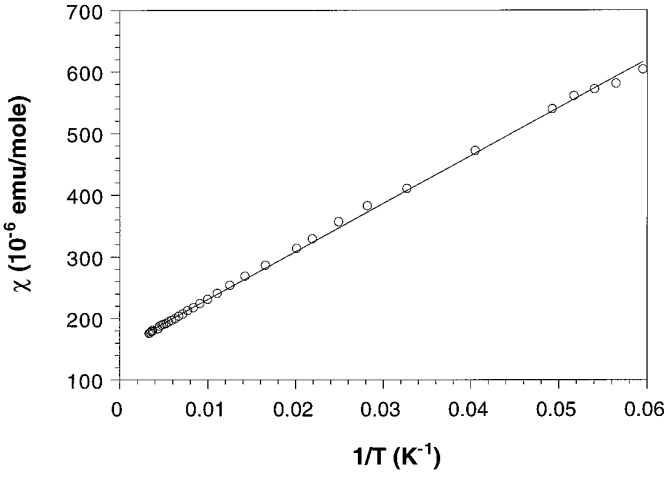

FIG. 7. Magnetic susceptibility versus inverse temperature for 600°C/24 h sample. The solid line through the data points is the least-square fit of the results based on Curie law with a temperature-independent constant term: $\chi = \chi_0 + C/T$. Analysis of the data gives an effective magnetic moment of 0.25 μ_B per vanadium.

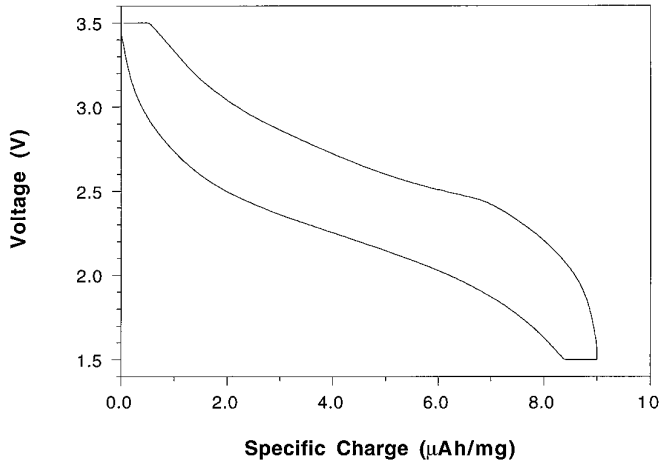

FIG. 8. One cycle of the single-phase cubic vanadium oxynitride cell with liquid electrolyte between 3.5 and 1.5 V at a constant current density of 200 μA/cm^2 at 25°C. The voltage was held constant until the current decreased to about 20 μA for both the discharge and recharge half cycle.

much smaller than that of the cell with the liquid electrolyte (Fig. 9). This loss of the capacity is probably due to the lack of good contact between cathode particles in the spin-coated composite cathode film. The decrease in voltage with increasing discharge current shown in Fig. 9 is due to the large internal resistance of the cell. Comparing the 1 and 20 μA/cm^2 curves in Fig. 9, this particular cell had a resistance of 42 KΩ near the midpoint of the discharge curve. Since the cubic vanadium oxynitride has a small electronic resistivity (2×10^{-3} $\Omega \cdot$cm), the major source of this large internal resistance of the cell is due to the slow diffusion of lithium ions into the close-packed NaCl

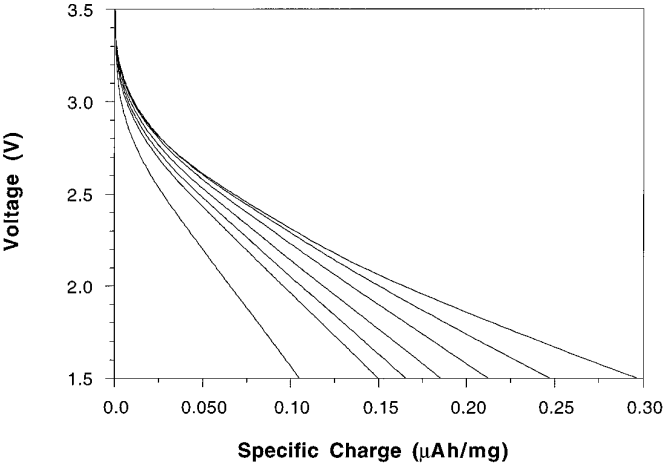

FIG. 9. Discharge curves of the single-phase cubic vanadium oxynitride cell with thin film solid electrolyte for different current densities at 25°C: 1, 2, 4, 6, 8, 10, and 20 μA/cm^2. The charge current density was 10 μA/cm^2. During the charge cycle, the voltage was held constant until the current decreased to about 1 μA.

structure. Nevertheless, the internal resistivity of this cell, $\sim 10^7$ $\Omega \cdot$cm, is comparable to that of thin film cells based on polycrystalline V_2O_5 cathodes, $\sim 10^7$ $\Omega \cdot$cm.

CONCLUSIONS

Single-phase cubic vanadium oxynitride can be prepared by nitridation of V_2O_5 at 600 to 700°C. The process of nitridation introduces lattice strain in the V(O,N) product, and this strain decreases with increasing processing temperature. Heavily doped semiconductor behavior was observed in the single-phase cubic vanadium oxynitride. The low capacity of the vanadium oxynitride cell indicates that only a small amount of lithium ions was inserted into the cathode due to the close-packed NaCl structure of cubic vanadium oxynitride.

ACKNOWLEDGMENTS

The authors thank Dr. N. J. Dudney for her critical reading of the manuscript, Dr. R. A. Zuhr for the RBS measurement, and Mr. C. F. Luck for his help in fabricating the thin film solid electrolyte cell for the electrochemical measurement. This research was sponsored by the Division of Materials Sciences, U. S. Department of Energy under contract No. DE-AC05-84OR21400 with Lockheed-Martin Marietta Energy Systems. BW was supported by an appointment to the Oak Ridge National Laboratory Postdoctoral Research Program administered by the Oak Ridge Institute for Science and Education.

REFERENCES

1. C. Delmas, H. Cognac-Auradou, J. M. Cocciantelli, M. Ménétrier, and J. P. Doumerc, *Solid State Ionics* **69,** 257 (1994).
2. K. West, B. Zachau-Christiansen, T. Jacobsen, and S. Skaarup, *Solid State Ionics* **76,** 15 (1995).
3. S. Erdei and F. W. Ainger, *Solid State Ionics* **68,** 295 (1994).
4. A. Shimizu, T. Tsumura, and M. Inagaki, *Solid State Ionics* **63–65,** 479 (1993).
5. B. Zachau-Christiansen, K. West, T. Jacobsen, and S. Skaarup, *Solid State Ionics* **53–56,** 364 (1992).
6. J. B. Bates, G. R. Gruzalski, N. J. Dudney, and C. F. Luck, *Proc. 35th Power Sources Symp.* 337 (1992).
7. J. B. Bates, N. J. Dudney, G. R. Gruzalski, C. F. Luck, X-H. Yu, and S. D. Jones, *Solid State Tech.* **July,** 59 (1993).
8. H. S. Kim, G. Bugli, G. Djega-Mariadassou, and M. Boudart, *in* "Synthesis and Properties of Advanced Catalytic Materials" (E. Iglesia, D. Nagaki, L. Thompson, and P. Lednor, Eds), Materials Research Society Symposium Proceedings, Vol. 368. Materials Research Society, Pittsburgh, 1994.
9. R. Marchand, X. Gouin, F. Tessier, and Y. Laurent, *in* "Synthesis and Properties of Advanced Catalytic Materials" (E. Iglesia, D. Nagaki, L. Thompson, and P. Lednor, Eds.), Materials Research Society Symposium Proceedings, Vol. 368. Materials Research Society, Pittsburgh, 1994.
10. A. A. Potorochin, G. P. Shveikin, and S. I. Alyamovskii, *Izv. Akad. Nauk SSR* **7,** 1355 (1970).
11. Von G. Brauer and H. Reuther, *Z. Anorg. Allg. Chem.* **395,** 151 (1973).
12. B. C. Chakoumakos, J. A. Fernandez-baca, and L. A. Boatner, *J. Solid State Chem.* **103,** 105 (1993).

13. A. C. Larson and R. B. Von Dreele, ''GSAS—General Structure Analysis System.'' Rept. LA-UR-86-748, Los Alamos National Laboratory, Los Alamos, NM 87545, 1990.
14. H. M. Rietveld, *J. Appl. Crystallogr.* **2,** 65 (1969).
15. B. C. Sales, E. C. Jones, B. C. Chakoumakos, J. A. Fernandez-baca, H. E. Harmon, J. W. Sharp, and E. I. Volckmann, *Phys. Rev. B* **50,** 8207 (1994).
16. M. D. Banus, T. B. Reed, and A. J. Strauss, *Phys. Rev. B* **5,** 2775 (1972).
17. J. I. Langford, D. Louer, E. J. Sonneveld, and J. W. Visser, *Powder Diff.* **1,** 211 (1986).
18. S. Kachi, T. Takada, Y. Bando, K. Kosuge, H. Okinaka, and K. Nagasawa, ''FERRITEs: Proceedings of the International Conference'' (Y. Hoshino, S. Iida, and M. Sugimoto, Eds.), p. 563. University Park Press, Baltimore/London/Tokyo, 1971.
19. R. M. Moon, *Phy.Rev. Lett.* **25,** 527 (1970).
20. A. F. Reid, T. M. Sabine, and D. A. Wheller, *J. Solid State Chem.* **4,** 400 (1972).
21. P. D. Dernier and M. Marezio, *Phys. Rev. B* **2,** 3771 (1970).
22. C. Kittel, ''Introduction to Solid State Physics.'' Wiley, New York, 1966.
23. J. B. Bates, N. J. Dudney, D. C. Lubben, G. R. Gruzalski, B. S. Kwak, X. Yu, and R. A. Zuhr, *J. Power Sources* **54,** 58 (1995).